Automatica 44 (2008) 2248–2257

Contents lists available at ScienceDirect

Automatica

journal homepage: www.elsevier.com/locate/automatica

Adaptive robust posture control of a parallel manipulator driven by pneumatic muscles☆

Xiaocong Zhu [a], Guoliang Tao [a,*], Bin Yao [a,b], Jian Cao [a]

[a] The State Key Laboratory of Fluid Power Transmission and Control, Zhejiang University, Hangzhou, 310027, China
[b] School of Mechanical Engineering, Purdue University, West Lafayette, IN 47907, USA

ARTICLE INFO

Article history:
Received 26 September 2006
Received in revised form
31 August 2007
Accepted 20 January 2008
Available online 12 March 2008

Keywords:
Pneumatic muscle
Parallel manipulator
Adaptive control
Nonlinear robust control

ABSTRACT

Rather severe parametric uncertainties and uncertain nonlinearities exist in the dynamic modeling of a parallel manipulator driven by pneumatic muscles. Those uncertainties not only come from the time-varying friction forces and the static force modeling errors of pneumatic muscles but also from the inherent complex nonlinearities and unknown disturbances of the parallel manipulator. In this paper, a discontinuous projection-based adaptive robust control strategy is adopted to compensate for both the parametric uncertainties and uncertain nonlinearities of a three-pneumatic-muscles-driven parallel manipulator to achieve precise posture trajectory tracking control. The resulting controller effectively handles the effects of various parameter variations and the hard-to-model nonlinearities such as the friction forces of the pneumatic muscles. Simulation and experimental results are obtained to illustrate the effectiveness of the proposed adaptive robust controller.

1. Introduction

Pneumatic muscle is a new type of flexible actuator similar to human muscle. It is usually made up of a rubber tube and cross-weave sheath material. Pneumatic muscles have the advantages of cleanness, cheapness, light-weight, easy maintenance, and the higher power/weight and power/volume ratios when compared with pneumatic cylinders (Ahn, Thanh, & Yang, 2004). The basic working principle of a pneumatic muscle is as follows: when the rubber tube is inflated, the cross-weave sheath experiences lateral expansion, resulting in axial contractive force and the movement of the end point position of the pneumatic muscle. Thus, the position or force control of a pneumatic muscle along its axial direction can be realized by regulating the inner pressure of its rubber tube. The parallel manipulator driven by pneumatic muscles (PMDPM) studied in this paper is a new application of pneumatic muscles. It consists of three pneumatic muscles connecting the moving arm of the parallel manipulator to its base platform as shown in Fig. 1. By controlling the lengths of three pneumatic muscles, three degrees-of-freedom (DOF) rotation motion of the parallel manipulator can be realized. Such a parallel manipulator combines the advantages of compact structure of parallel mechanisms with the adjustable stiffness and high power/volume ratio of pneumatic muscles, which will have promising wide applications in robotics, industrial automation, and bionic devices.

Many researchers have investigated the precise position control of pneumatic muscles during the past several years. Most of them dealt with the control of single or antagonistic pneumatic muscles. Specifically, Bowler, Caldwell, and Medrano-Cerda (1996), employed an adaptive pole-placement scheme to control a bi-directional pneumatic muscle actuator system, for use on a 7-DOF anthropomorphic robot arm. Cai and Yamaura (1996) presented a sliding mode controller for a manipulator driven by artificial muscle actuators. Kimura, Hara, Fujita, and Kagawa (1997), applied the feedback linearization method to the position control of a single-input pneumatic system with a third-order dynamics including the pressure dynamics. Kimoto and Ito (2003) added nonlinear robust compensations to a linear controller in order to stabilize the system globally and achieve robustness to uncertain nonlinearities. Carbonell, Jiang, and Repperger (2001), Chan, Lilly, Repperger, and Berlin (2003), Repperger, Johnson, and Phillips (1998) and Repperger, Phillips, and Krier (1999), proposed several methods such as fuzzy backstepping, gain-scheduling, variable structure and fuzzy PD+I for a SISO pneumatic muscle system with a second-order dynamics to achieve asymptotic position tracking. Lilly (2003), Lilly and Quesada (2004) and Lilly and Yang (2005), applied the sliding mode control technique with

☆ Part of the paper has been presented at the 2006 IFAC Symposium on Mechatronic Systems, Heidelberg, Germany. This paper was recommended for publication in revised form by Associate Editor Reza Katebi under the direction of Editor Mituhiko Araki. This work was supported by the National Natural Science Foundation of China (No. 50775200).

* Corresponding author. Tel.: +86 571 87951318; fax: +86 571 87951941.
E-mail addresses: zhuxiaoc@zju.edu.cn (X. Zhu), gltao@zju.edu.cn (G. Tao), byao@purdue.edu (B. Yao), caojianjiaowang@sina.com (J. Cao).

0005-1098/$ – see front matter © 2008 Elsevier Ltd. All rights reserved.
doi:10.1016/j.automatica.2008.01.015

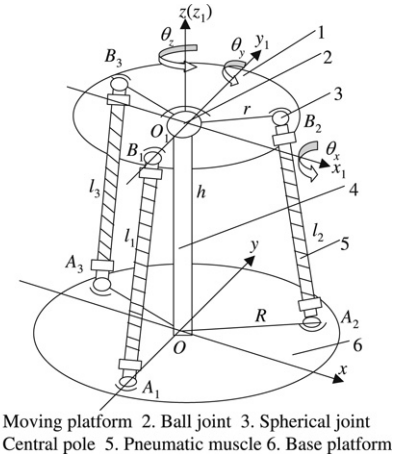

Fig. 1. Structure of the PMDPM.

boundary layer to control pneumatic muscle actuators arranged in bicep and tricep configurations. Tian, Ding, Yang, and Lin (2004), adopted the RPE algorithm to train neural networks for modeling and controlling an artificial muscle system. Hildebrandt, Sawodny, Neumann, and Hartmann (2002); Sawodny, Neumann, and Hartmann (2005), presented a cascade controller for a two-axis planar articulated robotic arm driven by four pneumatic muscles.

As reviewed above, some of the researchers designed robust controllers without considering the pressure dynamics, while the effect of pressure dynamics is essential for the precise control of pneumatic muscles (Carbonell et al., 2001; Chan et al., 2003; Lilly, 2003; Lilly & Quesada, 2004; Lilly & Yang, 2005; Repperger et al., 1998, 1999). Some of the researchers developed controllers with the assumption that the system model is accurate, or that model uncertainties satisfy matching condition only, while those assumptions are hard to be satisfied in practice (Hildebrandt et al., 2002, 2005; Kimura et al., 1997). For the PMDPM shown in Fig. 1, it not only has all the control difficulties associated with the pneumatic muscles, but also the added difficulties of the coupled multi-input-multi-output (MIMO) complex dynamics of the parallel manipulator and the large extent of unmatched model uncertainties of the combined overall system. In other words, there exist rather severe parametric uncertainties and uncertain nonlinearities, which are caused not only by the time-varying friction forces and static force modeling errors of pneumatic muscles but also by the inherent complex nonlinearities and unknown disturbances of the parallel manipulator. Therefore, it is very difficult to control precisely the posture of the PMDPM.

The recently proposed adaptive robust control (ARC) has been shown to be a very effective control strategy for systems with both parametric uncertainties and uncertain nonlinearities (Xu & Yao, 2001; Yao, 2003; Yao, Bu, Reedy, & Chiu, 2000; Yao & Tomizuka, 2001). This approach effectively integrates adaptive control with robust control through utilizing on-line parameter adaptation to reduce the extent of parametric uncertainties and employing certain robust control laws to attenuate the effects of various uncertainties. In ARC, a projection-type parameter estimation algorithm is used to solve the design conflict between adaptive control and robust control. Thus, high final tracking accuracy is achieved while guaranteeing excellent transient performance.

In this paper, the posture control of a PMDPM shown in Fig. 1 is considered in which each pneumatic muscle is controlled by two fast switching valves. The adaptive robust control strategy is applied to reduce the lumped uncertain nonlinearities and parametric uncertainties while using certain robust feedback to attenuate the effects of uncompensated model uncertainties. In addition, pressure dynamics are explicitly considered in the proposed controller. Consequently, good tracking performance is achieved in practice as demonstrated by simulation and experimental results.

The paper is organized as follows: Section 2 gives the dynamic models of the PMDPM controlled by fast switching valves. Section 3 presents the proposed adaptive robust controller, along with proofs of the stability and asymptotic output tracking of the resulting closed-loop system. Section 4 shows the advantages of the proposed adaptive robust controller over the traditional deterministic robust controller via simulation results. Section 5 details the obtained experimental results to verify the effectiveness of the proposed adaptive robust posture controller and Section 6 draws the conclusions.

2. Dynamic models

The PMDPM shown in Fig. 1 consists of a moving platform, a base platform, a central pole, and three pneumatic muscles. Pneumatic muscles are linked with the moving platform and the base platform by spherical joints B_i and A_i $(i = 1, 2, 3)$ respectively. The joints are evenly distributed along a circle on the moving platform and the base platform respectively. The central pole is rigidly fixed with the base platform and is connected with the moving platform by a ball joint. Consider two frames, the first one, reference frame *Oxyz* fixed to the base platform, and the second one, moving frame $O_1x_1y_1z_1$ attached to the moving platform at the center (Tao, Zhu, & Cao, 2005). The posture of the PMDPM is defined through the standard Roll–Pitch–Yaw (RPY) angles: first rotate the moving frame around the fixed x-axis by the yaw angle θ_x, then rotate the moving frame around the fixed y-axis by the pitch angle θ_y, and finally rotate the moving frame around the fixed z-axis by the roll angle θ_z. Two fast switching valves are used to regulate the pressure inside each pneumatic muscle, and this combination is subsequently referred to as a driving unit.

Some realistic assumptions are made as follows to simplify the analysis: (a) The working medium of the pneumatic muscles satisfies the ideal gas equation, (b) Resistance and dynamics of various pipes of the pneumatic muscles are neglected, (c) The gas leakage from the pipe is neglected, and (d) The opening and closing time of the fast switching valves are also neglected.

2.1. Dynamic model of parallel manipulator

2.1.1. Inverse kinematics of parallel manipulator

Let the posture vector of the moving platform be $\boldsymbol{\theta} = [\theta_x, \theta_y, \theta_z]^{\mathrm{T}}$. Define $\boldsymbol{P}_{\mathrm{A}i} \in R^3$ as the position vector of the ith spherical joint of the base platform in frame *Oxyz* and $\boldsymbol{P}_{\mathrm{b}i} \in R^3$ as the position vector of the ith spherical joint of the moving platform in frame $O_1x_1y_1z_1$. Let $\boldsymbol{T}_{\mathrm{h}} \in R^3$ be the position vector of the center O_1 in frame *Oxyz* and $\boldsymbol{P}_{\mathrm{B}i}$ the position vector of the ith spherical joint of the moving platform in frame *Oxyz*. Then,

$$\boldsymbol{P}_{\mathrm{B}i}(\boldsymbol{\theta}) = \boldsymbol{R}_0(\boldsymbol{\theta})\boldsymbol{P}_{\mathrm{b}i} + \boldsymbol{T}_{\mathrm{h}} \tag{1}$$

where $\boldsymbol{R}_0(\boldsymbol{\theta})$ is the rotational matrix from frame $O_1x_1y_1z_1$ to frame *Oxyz* and was uniquely determined using the posture vector $\boldsymbol{\theta}$ by Huang, Kou, and Fang (1997)

$$\boldsymbol{R}_0(\boldsymbol{\theta}) = \begin{bmatrix} c\theta_z c\theta_y & c\theta_z s\theta_y s\theta_x - s\theta_z c\theta_x & c\theta_z s\theta_y c\theta_x + s\theta_z s\theta_x \\ s\theta_z c\theta_y & s\theta_z s\theta_y s\theta_x + c\theta_z c\theta_x & s\theta_z s\theta_y c\theta_x - c\theta_z s\theta_x \\ -s\theta_y & c\theta_y s\theta_x & c\theta_y c\theta_x \end{bmatrix} \tag{2}$$

where $c\theta$ and $s\theta$ are short-hand notations for $\cos\theta$ and $\sin\theta$ respectively. The contractive length of the ith pneumatic muscle $x_{\mathrm{m}i}$ can then be determined as

$$x_{\mathrm{m}i}(\boldsymbol{\theta}) = L_0 + L_{\mathrm{J}i} - |\boldsymbol{P}_{\mathrm{A}i} - \boldsymbol{P}_{\mathrm{B}i}(\boldsymbol{\theta})|, \quad i = 1, 2, 3 \tag{3}$$

where L_0 is the initial length of pneumatic muscle, L_{ji} is the ineffective length between the base platform and the moving platform excluding the effective length of the ith pneumatic muscle, and $|\bullet|$ represents the Euclidean norm of a vector. Eq. (3) solves the inverse kinematics of the moving platform from the posture vector $\boldsymbol{\theta}$ to the contractive length vector of three pneumatic muscles $\boldsymbol{x}_{\mathrm{m}} = [x_{\mathrm{m1}}, x_{\mathrm{m2}}, x_{\mathrm{m3}}]^{\mathrm{T}}$.

2.1.2. Dynamics of parallel manipulator

Let F_i be the value of the force acting on the moving platform by the ith pneumatic muscle along its axial direction, with positive value for the contractive force. Denote a force vector as $\boldsymbol{F} = [F_1, F_2, F_3]^{\mathrm{T}}$. Let the angular velocity of the moving platform expressed in the base frame $Oxyz$ be $\boldsymbol{\omega} \in R^3$. Then, according to the dynamic equation of a rigid body, the dynamic model of the moving platform can be written as Tao et al. (2005)

$$\boldsymbol{I}(\boldsymbol{\theta})\dot{\boldsymbol{\omega}} + \boldsymbol{C}(\boldsymbol{\theta}, \dot{\boldsymbol{\theta}})\boldsymbol{\omega} + \boldsymbol{C}_{\mathrm{s}}\boldsymbol{\omega} + \tilde{\boldsymbol{\delta}}(t) = \boldsymbol{J}^{\mathrm{T}}(\boldsymbol{\theta})\boldsymbol{F} \tag{4}$$

where $\boldsymbol{I}(\boldsymbol{\theta})$ is the rotational inertia matrix and $\boldsymbol{C}(\boldsymbol{\theta}, \dot{\boldsymbol{\theta}})\boldsymbol{\omega}$ represents the Coriolis terms, $\boldsymbol{C}_{\mathrm{s}} = \mathrm{diag}([c_{s1}, c_{s2}, c_{s3}]^{\mathrm{T}})$ represents the coefficient matrix of viscous frictions of the spherical joints, $\tilde{\boldsymbol{\delta}}(t) = [\tilde{\delta}_x, \tilde{\delta}_y, \tilde{\delta}_z]^{\mathrm{T}}$ represents the external disturbance vector, and $\boldsymbol{J}(\boldsymbol{\theta})$ is the Jacobian transformation matrix between the contractive velocity vector of pneumatic muscles and angular velocity vector of the moving platform.

The dynamic equations of the driving units can be written as

$$\boldsymbol{M}\ddot{\boldsymbol{x}}_{\mathrm{m}} + \boldsymbol{F}_{\mathrm{f}} + \boldsymbol{F} = \boldsymbol{F}_{\mathrm{m}} \tag{5}$$

where $\boldsymbol{M} = \mathrm{diag}([m_1, m_2, m_3]^{\mathrm{T}})$ is the equivalent mass matrix of three pneumatic muscles and their spherical joints, $\boldsymbol{F}_{\mathrm{f}} = [F_{\mathrm{f1}}, F_{\mathrm{f2}}, F_{\mathrm{f3}}]^{\mathrm{T}}$ is the friction force vector of pneumatic muscles, and $\boldsymbol{F}_{\mathrm{m}} = [F_{\mathrm{m1}}, F_{\mathrm{m2}}, F_{\mathrm{m3}}]^{\mathrm{T}}$ is the static force vector of pneumatic muscles detailed in Section 2.2. Merging Eqs. (4) and (5) while noting $\dot{\boldsymbol{x}}_{\mathrm{m}} = \boldsymbol{J}(\boldsymbol{\theta})\boldsymbol{\omega}$ and $\dot{\boldsymbol{\theta}} = \boldsymbol{G}^{-1}(\boldsymbol{\theta})\boldsymbol{\omega}$ in which $\boldsymbol{G}(\boldsymbol{\theta})$ is the transformation matrix from the angular velocity vector to the posture velocity vector of the PMDPM via three RPY angles, the dynamic model of PMDPM can be obtained as follows in terms of posture vector.

$$\boldsymbol{I}_{\mathrm{p}}(\boldsymbol{\theta})\ddot{\boldsymbol{\theta}} + \boldsymbol{B}_{\mathrm{p}}(\boldsymbol{\theta})\dot{\boldsymbol{\theta}} + \boldsymbol{d}_{\mathrm{t}}(\boldsymbol{\theta}, \dot{\boldsymbol{\theta}}, t) = \boldsymbol{J}_{\theta}^{\mathrm{T}}(\boldsymbol{\theta})\boldsymbol{F}_{\mathrm{m}} \tag{6}$$

where $\boldsymbol{I}_{\mathrm{p}}(\boldsymbol{\theta}) = \boldsymbol{G}^{\mathrm{T}}(\boldsymbol{\theta})[\boldsymbol{I}(\boldsymbol{\theta}) + \boldsymbol{J}^{\mathrm{T}}(\boldsymbol{\theta})\boldsymbol{M}\boldsymbol{J}(\boldsymbol{\theta})]\boldsymbol{G}(\boldsymbol{\theta})$, $\boldsymbol{B}_{\mathrm{p}}(\boldsymbol{\theta}) = \boldsymbol{G}^{\mathrm{T}}(\boldsymbol{\theta})\boldsymbol{C}_{\mathrm{s}}\boldsymbol{G}(\boldsymbol{\theta})$, $\boldsymbol{d}_{\mathrm{t}}(\boldsymbol{\theta}, \dot{\boldsymbol{\theta}}, t) = \boldsymbol{G}^{\mathrm{T}}(\boldsymbol{\theta})\boldsymbol{I}(\boldsymbol{\theta})\dot{\boldsymbol{G}}(\boldsymbol{\theta}, \dot{\boldsymbol{\theta}})\dot{\boldsymbol{\theta}} + \boldsymbol{G}^{\mathrm{T}}(\boldsymbol{\theta})\boldsymbol{J}^{\mathrm{T}}(\boldsymbol{\theta})\boldsymbol{M}\dot{\boldsymbol{J}}(\boldsymbol{\theta})\dot{\boldsymbol{G}}(\boldsymbol{\theta}, \dot{\boldsymbol{\theta}})\dot{\boldsymbol{\theta}} + \boldsymbol{G}^{\mathrm{T}}(\boldsymbol{\theta})\boldsymbol{C}(\boldsymbol{\theta}, \dot{\boldsymbol{\theta}})\boldsymbol{G}(\boldsymbol{\theta})\dot{\boldsymbol{\theta}} + \boldsymbol{G}^{\mathrm{T}}(\boldsymbol{\theta})\boldsymbol{J}^{\mathrm{T}}(\boldsymbol{\theta})\boldsymbol{M}\dot{\boldsymbol{J}}(\boldsymbol{\theta}, \dot{\boldsymbol{\theta}})\boldsymbol{G}(\boldsymbol{\theta})\dot{\boldsymbol{\theta}} + \boldsymbol{G}^{\mathrm{T}}(\boldsymbol{\theta})\boldsymbol{J}^{\mathrm{T}}(\boldsymbol{\theta})\boldsymbol{F}_{\mathrm{f}} + \boldsymbol{G}^{\mathrm{T}}(\boldsymbol{\theta})\tilde{\boldsymbol{\delta}}(t)$, $\boldsymbol{J}_{\theta}(\boldsymbol{\theta}) = \boldsymbol{J}(\boldsymbol{\theta})\boldsymbol{G}(\boldsymbol{\theta})$.

2.2. Models of actuator

2.2.1. Characteristics of pneumatic muscle

For each driving unit i, the static force of pneumatic muscle is (Chou & Hannaford, 1996; Tondu & Lopez, 2000; Yang, Li, & Liu, 2002)

$$F_{\mathrm{mi}}(x_{\mathrm{mi}}, p_i) = p_i[a(1 - k_{\varepsilon}\varepsilon_{\mathrm{mi}})^2 - b] - F_{\mathrm{ri}}(x_{\mathrm{mi}}) + \delta_{\mathrm{Fi}} \tag{7}$$

$$F_{\mathrm{ri}}(x_{\mathrm{mi}}) = \pi D_0 L_0 \delta_0 E(1 - \varepsilon_{\mathrm{mi}})^2 \times \left(\frac{1}{\sin\alpha_0} - \frac{1}{\sin\alpha_i(x_{\mathrm{mi}})}\right)\cos\alpha_0 \tag{8}$$

where p_i is the pressure inside the pneumatic muscle, a and b are constants related to the structure of pneumatic muscle, k_{ε} is a factor accounting for the side effect, $\varepsilon_{\mathrm{mi}}$ is the contractive ratio given by $\varepsilon_{\mathrm{mi}} = x_{\mathrm{mi}}/L_0$, $F_{\mathrm{ri}}(x_{\mathrm{mi}})$ is the rubber elastic force, D_0 is the initial diameter of the pneumatic muscle, δ_0 is the thickness of shell and bladder, E is the bulk modulus of elasticity of rubber tube with cross-weave sheath, α_0 is the initial braided angle of the pneumatic muscle, $\alpha_i(x_{\mathrm{mi}})$ is the current braided angle of the pneumatic muscle given by $\alpha_i(x_{\mathrm{mi}}) = \arccos[(L_0 - x_{\mathrm{mi}})\cos\alpha_0/L_0]$, and δ_{Fi} is the modeling error.

2.2.2. Actuator dynamics

The pressure dynamics that generates the pressure inside the pneumatic muscle will be given. Suppose the relationship between volume and pressure inside the pneumatic muscle can be described by polytropic gas law

$$p_i\left(\frac{V_i(x_{\mathrm{mi}})}{m_{ai}}\right)^{\lambda_i} = \mathrm{const} \tag{9}$$

where $V_i(x_{\mathrm{mi}})$ is the pneumatic muscle's inner volume, which is a function of x_{mi}, m_{ai} is the air mass inside the pneumatic muscle, and λ_i is the polytropic exponent. The ideal gas equation describes the dependency of the air mass.

$$p_i V_i(x_{\mathrm{mi}}) = m_{ai} R T_i \tag{10}$$

where R is the gas constant and T_i is the thermodynamic temperature inside the pneumatic muscle.

Differentiate Eq. (9) while noting Eq. (10), one obtains

$$\dot{p}_i = \frac{\lambda_i R T_i \dot{m}_{ai}}{V_i(x_{\mathrm{mi}})} - \frac{\lambda_i p_i \dot{V}_i(x_{\mathrm{mi}}, \dot{x}_{\mathrm{mi}})}{V_i(x_{\mathrm{mi}})} \tag{11}$$

where $\dot{m}_{ai}$ is the air mass flow rate through the valve.

Suppose $\dot{m}_{ai} = C_q q_{\mathrm{mi}} + \tilde{q}_{\mathrm{mi}}(t)$ in which q_{mi} is the calculable air mass flow rate given in Section 2.2.3, C_q and $\tilde{q}_{\mathrm{mi}}(t)$ are the coefficient and disturbance considering model errors respectively. Then the following general pressure dynamic equation instead of Eq. (11) will be used (Richer & Hurmuzlu, 2000)

$$\dot{p}_i = \frac{\lambda_{bi} R T_i q_{\mathrm{mi}}}{V_i(x_{\mathrm{mi}})} - \frac{\lambda_{ai} p_i \dot{V}_i(x_{\mathrm{mi}}, \dot{x}_{\mathrm{mi}})}{V_i(x_{\mathrm{mi}})} + d_{\mathrm{q}i}(t) \tag{12}$$

where $\lambda_{ai} = \lambda_i$, $\lambda_{bi} = C_q\lambda_i$, and $d_{\mathrm{q}i}(t) = \frac{\lambda_i R T_i \tilde{q}_{\mathrm{mi}}(t)}{V_i(x_{\mathrm{mi}})}$.

2.2.3. Valve model

The relationship between the calculable air mass flow rate q_{mi} into the ith pneumatic muscle and control input u_i (the duty cycle of two fast switching valves in the ith driving unit) can be put into the following concise form (Tao et al., 2005)

$$q_{\mathrm{mi}}(u_i) = K_{\mathrm{q}i}(p_i, \mathrm{sign}(u_i))u_i \tag{13}$$

where $K_{\mathrm{q}i}$ is a nonlinear flow gain function given by $K_{\mathrm{q}i}(p_i, \mathrm{sign}(u_i)) = A_{\mathrm{e}i}\frac{p_{\mathrm{u}i}}{\sqrt{RT_{\mathrm{u}i}}} f(\frac{p_{\mathrm{d}i}}{p_{\mathrm{u}i}})$ with

$$f\left(\frac{p_{\mathrm{d}i}}{p_{\mathrm{u}i}}\right) = \begin{cases} \sqrt{k\left(\frac{2}{k+1}\right)^{\frac{k+1}{k-1}}} & \text{when } 0 \le \dfrac{p_{\mathrm{d}i}}{p_{\mathrm{u}i}} < 0.528 \\ \sqrt{\dfrac{2k}{k-1}\left[\left(\dfrac{p_{\mathrm{d}i}}{p_{\mathrm{u}i}}\right)^{\frac{2}{k}} - \left(\dfrac{p_{\mathrm{d}i}}{p_{\mathrm{u}i}}\right)^{\frac{k+1}{k}}\right]} & \text{when } 0.528 \le \dfrac{p_{\mathrm{d}i}}{p_{\mathrm{u}i}} \le 1 \end{cases}$$

in which $A_{\mathrm{e}i}$ is the effective orifice area of fast switching valve, $p_{\mathrm{u}i}$ is the upstream pressure, $p_{\mathrm{d}i}$ is the downstream pressure, $T_{\mathrm{u}i}$ is the upstream temperature and k is the ratio of specific heat.

2.3. Dynamics in state-space form

Let $\bar{\boldsymbol{F}}_{\mathrm{m}}(\boldsymbol{x}_{\mathrm{m}}, \boldsymbol{p}) = \boldsymbol{F}_{\mathrm{m}}(\boldsymbol{x}_{\mathrm{m}}, \boldsymbol{p}) - \boldsymbol{\delta}_{\mathrm{F}}$ be the calculable and differentiable part of $\boldsymbol{F}_{\mathrm{m}}$. And define the drive moment of the PMDPM in task-space as

$$\boldsymbol{\tau} = \boldsymbol{J}_{\theta}^{\mathrm{T}}(\boldsymbol{\theta})\bar{\boldsymbol{F}}_{\mathrm{m}}(\boldsymbol{x}_{\mathrm{m}}, \boldsymbol{p}). \tag{14}$$

Differentiate Eq. (14) while noting Eqs. (12) and (13), the dynamics of actuators are described as

$$\dot{\boldsymbol{\tau}} = \boldsymbol{f}_{\tau}(\boldsymbol{\theta}, \dot{\boldsymbol{\theta}}, \boldsymbol{p}) + \boldsymbol{g}_{\tau}(\boldsymbol{\theta})\boldsymbol{K}_{\mathrm{q}}(\boldsymbol{p}, \mathrm{sign}(\boldsymbol{u}))\boldsymbol{u} + \boldsymbol{d}_{\tau}(t) \tag{15}$$

where

$$\boldsymbol{f}_\tau(\boldsymbol{\theta},\dot{\boldsymbol{\theta}},\boldsymbol{p}) = \boldsymbol{J}_\theta^{\mathrm{T}}(\boldsymbol{\theta},\dot{\boldsymbol{\theta}})\bar{\boldsymbol{F}}_{\mathrm{m}}(\boldsymbol{x}_{\mathrm{m}},\boldsymbol{p}) + \boldsymbol{J}_\theta^{\mathrm{T}}(\boldsymbol{\theta})\frac{\partial \bar{\boldsymbol{F}}_{\mathrm{m}}(\boldsymbol{x}_{\mathrm{m}},\boldsymbol{p})}{\partial \boldsymbol{x}_{\mathrm{m}}}\dot{\boldsymbol{x}}_{\mathrm{m}} - \boldsymbol{J}_\theta^{\mathrm{T}}(\boldsymbol{\theta})\frac{\partial \bar{\boldsymbol{F}}_{\mathrm{m}}(\boldsymbol{x}_{\mathrm{m}},\boldsymbol{p})}{\partial \boldsymbol{p}}\boldsymbol{A}_f(\boldsymbol{x}_{\mathrm{m}},\dot{\boldsymbol{x}}_{\mathrm{m}},\boldsymbol{p})\boldsymbol{\lambda}_a, \boldsymbol{A}_f(\boldsymbol{x}_{\mathrm{m}},\dot{\boldsymbol{x}}_{\mathrm{m}},\boldsymbol{p})$$

$$= \mathrm{diag}\left(\left[\frac{p_1\dot{V}_1(x_{\mathrm{m1}},\dot{x}_{\mathrm{m1}})}{V_1(x_{\mathrm{m1}})}, \frac{p_2\dot{V}_2(x_{\mathrm{m2}},\dot{x}_{\mathrm{m2}})}{V_2(x_{\mathrm{m2}})}, \frac{p_3\dot{V}_3(x_{\mathrm{m3}},\dot{x}_{\mathrm{m3}})}{V_3(x_{\mathrm{m3}})}\right]^{\mathrm{T}}\right),$$

$$\boldsymbol{g}_\tau(\boldsymbol{\theta}) = \boldsymbol{J}_\theta^{\mathrm{T}}(\boldsymbol{\theta})\frac{\partial \bar{\boldsymbol{F}}_{\mathrm{m}}(\boldsymbol{x}_{\mathrm{m}},\boldsymbol{p})}{\partial \boldsymbol{p}}\boldsymbol{A}_g(\boldsymbol{x}_{\mathrm{m}})\mathrm{diag}(\boldsymbol{\lambda}_b),$$

$$\boldsymbol{A}_g(\boldsymbol{x}_{\mathrm{m}}) = \mathrm{diag}\left(\left[\frac{RT_1}{V_1(x_{\mathrm{m1}})}, \frac{RT_2}{V_2(x_{\mathrm{m2}})}, \frac{RT_3}{V_3(x_{\mathrm{m3}})}\right]^{\mathrm{T}}\right),$$

$$\boldsymbol{d}_\tau(t) = \boldsymbol{J}_\theta^{\mathrm{T}}(\boldsymbol{\theta})\frac{\partial \bar{\boldsymbol{F}}_{\mathrm{m}}(\boldsymbol{x}_{\mathrm{m}},\boldsymbol{p})}{\partial \boldsymbol{p}}\boldsymbol{d}_{\mathrm{q}}(t), \boldsymbol{d}_{\mathrm{q}} = [d_{\mathrm{q1}}, d_{\mathrm{q2}}, d_{\mathrm{q3}}]^{\mathrm{T}},$$

$$\frac{\partial \bar{\boldsymbol{F}}_{\mathrm{m}}(\boldsymbol{x}_{\mathrm{m}},\boldsymbol{p})}{\partial \boldsymbol{p}} = \mathrm{diag}\left(\left[\frac{\partial \bar{F}_{\mathrm{m1}}(x_{\mathrm{m1}},p_1)}{\partial p_1}, \frac{\partial \bar{F}_{\mathrm{m2}}(x_{\mathrm{m2}},p_2)}{\partial p_2}, \frac{\partial \bar{F}_{\mathrm{m3}}(x_{\mathrm{m3}},p_3)}{\partial p_3}\right]^{\mathrm{T}}\right),$$

$$\frac{\partial \bar{\boldsymbol{F}}_{\mathrm{m}}(\boldsymbol{x}_{\mathrm{m}},\boldsymbol{p})}{\partial \boldsymbol{x}_{\mathrm{m}}} = \mathrm{diag}\left(\left[\frac{\partial \bar{F}_{\mathrm{m1}}(x_{\mathrm{m1}},p_1)}{\partial x_{\mathrm{m1}}}, \frac{\partial \bar{F}_{\mathrm{m2}}(x_{\mathrm{m2}},p_2)}{\partial x_{\mathrm{m2}}}, \frac{\partial \bar{F}_{\mathrm{m3}}(x_{\mathrm{m3}},p_3)}{\partial x_{\mathrm{m3}}}\right]^{\mathrm{T}}\right),$$

$$\boldsymbol{K}_{\mathrm{q}}(\boldsymbol{p},\mathrm{sign}(\boldsymbol{u})) = \mathrm{diag}([K_{\mathrm{q1}}(p_1,\mathrm{sign}(u_1)), K_{\mathrm{q2}}(p_2,\mathrm{sign}(u_2)), K_{\mathrm{q3}}(p_3,\mathrm{sign}(u_3))]^{\mathrm{T}}),$$

$$\boldsymbol{u} = [u_1,u_2,u_3]^{\mathrm{T}}, \boldsymbol{p} = [p_1,p_2,p_3]^{\mathrm{T}}, \boldsymbol{\lambda}_a = [\lambda_{a1},\lambda_{a2},\lambda_{a3}]^{\mathrm{T}},$$

$$\boldsymbol{\lambda}_b = [\lambda_{b1},\lambda_{b2},\lambda_{b3}]^{\mathrm{T}}.$$

Define a set of state variables as $\boldsymbol{x} = [\boldsymbol{x}_1^{\mathrm{T}}, \boldsymbol{x}_2^{\mathrm{T}}, \boldsymbol{x}_3^{\mathrm{T}}]^{\mathrm{T}} = [\boldsymbol{\theta}^{\mathrm{T}}, \dot{\boldsymbol{\theta}}^{\mathrm{T}}, \boldsymbol{\tau}^{\mathrm{T}}]^{\mathrm{T}}$. Then the entire system can be expressed in a state-space form as

$$\begin{cases} \dot{\boldsymbol{x}}_1 = \boldsymbol{x}_2 \\ \dot{\boldsymbol{x}}_2 = \boldsymbol{I}_{\mathrm{p}}^{-1}(\boldsymbol{x}_1)[\boldsymbol{x}_3 - \boldsymbol{B}_{\mathrm{p}}(\boldsymbol{x}_1)\boldsymbol{x}_2 - \boldsymbol{d}_{\mathrm{p}}] \\ \dot{\boldsymbol{x}}_3 = \dot{\boldsymbol{f}}_\tau(\boldsymbol{x}_1,\boldsymbol{x}_2,\boldsymbol{f}_{\mathrm{p}}(\boldsymbol{x}_1,\boldsymbol{x}_3)) + \boldsymbol{g}_\tau(\boldsymbol{x}_1)\boldsymbol{K}_{\mathrm{q}}\boldsymbol{u} + \dot{\boldsymbol{d}}_\tau \end{cases} \tag{16}$$

where $\boldsymbol{f}_{\mathrm{p}}(\boldsymbol{x}_1,\boldsymbol{x}_3)$ is the inverse function of Eq. (14) from $\boldsymbol{\tau}$ to $\boldsymbol{p}$, and $\boldsymbol{d}_{\mathrm{p}} = \boldsymbol{d}_{\mathrm{t}}(\boldsymbol{\theta},\dot{\boldsymbol{\theta}},t) - \boldsymbol{J}_\theta^{\mathrm{T}}(\boldsymbol{\theta})\delta_{\mathrm{F}}$. Note that both $\boldsymbol{I}_{\mathrm{p}}(\boldsymbol{x}_1)$ and $\boldsymbol{g}_\tau(\boldsymbol{x}_1)$ are positive definite matrices. For the simplicity of notation, the variables such as $\boldsymbol{J}_\theta(\boldsymbol{\theta})$ and $\boldsymbol{I}_{\mathrm{p}}(\boldsymbol{\theta})$ are expressed by $\boldsymbol{J}_\theta$ and $\boldsymbol{I}_{\mathrm{p}}$ when no confusions on the function variables exist.

3. Adaptive robust controller

3.1. Design issues to be addressed

Generally the system is subjected to parametric uncertainties due to the variation of $\boldsymbol{C}_s, \boldsymbol{I}_{\mathrm{p}}, \boldsymbol{\lambda}_a, \boldsymbol{\lambda}_b$ etc., and uncertain nonlinearities represented by $\boldsymbol{d}_{\mathrm{p}}$ and $\boldsymbol{d}_\tau$ that come from uncompensated model terms due to complex computation, unknown model errors and disturbances etc. Practically, $\boldsymbol{d}_{\mathrm{p}}$ and $\boldsymbol{d}_\tau$ may be decomposed into two parts, the constant or slowly changing part denoted by $\boldsymbol{d}_{\mathrm{pn}}$ and $\boldsymbol{d}_{\tau\mathrm{n}}$, and the fast changing part denoted by $\tilde{\boldsymbol{d}}_{\mathrm{p}}$ and $\tilde{\boldsymbol{d}}_\tau$, i.e., $\boldsymbol{d}_{\mathrm{p}} = \boldsymbol{d}_{\mathrm{pn}} + \tilde{\boldsymbol{d}}_{\mathrm{p}}$, $\boldsymbol{d}_\tau = \boldsymbol{d}_{\tau\mathrm{n}} + \tilde{\boldsymbol{d}}_\tau$. The main unknown parameters will be updated on-line through adaptation law to improve performance while the effects of other minor parameters will be lumped into uncertain nonlinearities. For simplicity, the following notations are used throughout the paper: $\bullet_i$ is used for the ith component of the vector $\bullet$, the operation $\leq$ for two vectors is performed in terms of the corresponding elements of the vectors, and $\boldsymbol{\beta}$ denotes the uncertain parameter vector. Then, the following assumption is made as in Yao et al. (2000).

Assumption: The extent of parametric uncertainties and uncertain nonlinearities are known, i.e., $\boldsymbol{\beta} \in \Omega_\beta = \{\boldsymbol{\beta} : \boldsymbol{\beta}_{\min} \leq \boldsymbol{\beta} \leq \boldsymbol{\beta}_{\max}\}$, $|\tilde{\boldsymbol{d}}_{\mathrm{p}}| \leq \boldsymbol{d}_{\mathrm{pmax}}$, $|\tilde{\boldsymbol{d}}_\tau| \leq \boldsymbol{d}_{\tau\max}$, where $\boldsymbol{\beta}_{\max} = [\beta_{1\max},\ldots,\beta_{n\max}]^{\mathrm{T}}$ is the maximum parameter vector, $\boldsymbol{\beta}_{\min} = [\beta_{1\min},\ldots,\beta_{n\min}]^{\mathrm{T}}$ is the minimum parameter vector, $\boldsymbol{d}_{\mathrm{pmax}}$ and $\boldsymbol{d}_{\tau\max}$ are known vectors.

It can be seen that the major difficulties in controlling are:

(a) The entire system is a highly nonlinear MIMO coupling dynamic system, due to either unknown disturbances $\boldsymbol{d}_{\mathrm{p}}$, $\boldsymbol{d}_\tau$ and nonlinear flow gains $\boldsymbol{K}_{\mathrm{q}}(\boldsymbol{p},\mathrm{sign}(\boldsymbol{u}))$ or nonlinear and time-varying terms such as $\boldsymbol{B}_{\mathrm{p}}(\boldsymbol{x}_1)$. Therefore, it is more suitable to design a nonlinear controller based on the MIMO model instead of a linear controller based on linearization.

(b) The system has severe parametric uncertainties represented by the lack of knowledge of damping coefficients $\boldsymbol{C}_{\mathrm{s}}$ and the polytropic exponents $\boldsymbol{\lambda}_a$ and $\boldsymbol{\lambda}_b$. Hence on-line parameter adaptation method should be adopted to reduce parametric uncertainties.

(c) The system has large extent of lumped modeling errors like unknown disturbances and unmodeled friction forces, which are contained in $\boldsymbol{d}_{\mathrm{p}}$ and $\boldsymbol{d}_\tau$. So both on-line adaptation and effective robust attenuation to these terms should be used for good control performance.

(d) The model uncertainties are unmatched, i.e., both parametric uncertainties and uncertain nonlinearities appear in the dynamic equations of the PMDPM that are not directly related to the control input $\boldsymbol{u}$. Therefore, the backstepping design technology should be employed to overcome design difficulties for achieving asymptotic stability.

3.2. Projection mapping

Let $\hat{\boldsymbol{\beta}}$ denote the estimate of $\boldsymbol{\beta}$ and $\tilde{\boldsymbol{\beta}} = \hat{\boldsymbol{\beta}} - \boldsymbol{\beta}$ the estimation error. In view of **Assumption**, the following projection-type parameter adaptation law is used to guarantee that the parameter estimates remain in the known bounded region all the time (Yao et al., 2000).

$$\dot{\hat{\boldsymbol{\beta}}} = \mathrm{Proj}_{\hat{\boldsymbol{\beta}}}(\boldsymbol{\Gamma}\boldsymbol{\sigma}), \qquad \hat{\boldsymbol{\beta}}(0) \in \Omega_\beta \tag{17}$$

$$\mathrm{Proj}_{\hat{\boldsymbol{\beta}}}(\bullet_i) = \begin{cases} 0 & \text{if } \hat{\beta}_i = \beta_{i\max} \text{ and } \bullet_i > 0 \\ 0 & \text{if } \hat{\beta}_i = \beta_{i\min} \text{ and } \bullet_i < 0 \\ \bullet_i & \text{otherwise} \end{cases} \tag{18}$$

where $\boldsymbol{\Gamma}$ is a positive definite diagonal matrix of adaptation rates and $\boldsymbol{\sigma}$ is a parameter adaptation function to be synthesized later. It can be shown that for any adaptation function, such a parameter adaptation law guarantees

$$\begin{cases} \hat{\boldsymbol{\beta}} \in \Omega_\beta = \{\hat{\boldsymbol{\beta}} : \boldsymbol{\beta}_{\min} \leq \hat{\boldsymbol{\beta}} \leq \boldsymbol{\beta}_{\max}\} \\ \tilde{\boldsymbol{\beta}}^{\mathrm{T}}[\boldsymbol{\Gamma}^{-1}\mathrm{Proj}_{\hat{\boldsymbol{\beta}}}(\boldsymbol{\Gamma}\boldsymbol{\sigma}) - \boldsymbol{\sigma}] \leq 0, \quad \forall \boldsymbol{\sigma}. \end{cases} \tag{19}$$

3.3. ARC controller design

The design is carried out using the recursive backstepping design procedure via ARC Lyapunov functions in task-space and muscle-space as follows (Yao et al., 2000).

(1) Step 1

Define a switching-function-like quantity as

$$\boldsymbol{z}_2 = \dot{\boldsymbol{z}}_1 + \boldsymbol{K}_{\mathrm{c}}\boldsymbol{z}_1 \tag{20}$$

where $\boldsymbol{z}_1 = \boldsymbol{x}_1 - \boldsymbol{y}_\mathrm{d}$ is the trajectory tracking error vector and $\boldsymbol{K}_\mathrm{c}$ is a positive definite diagonal feedback matrix. If $\boldsymbol{z}_2$ converges to a small value or zero, then $\boldsymbol{z}_1$ will converge to a small value or zero since the transfer function from $\boldsymbol{z}_2$ to $\boldsymbol{z}_1$ is stable. Thus the next objective is to design the drive moment $\boldsymbol{\tau}$ for making $\boldsymbol{z}_2$ as small as possible. For this purpose, define the unknown parameter vector in task-space as $\boldsymbol{\beta}_\mathrm{t} = [c_{s1}, c_{s2}, c_{s3}, d_\mathrm{pnx}, d_\mathrm{pny}, d_\mathrm{pnz}]^\mathrm{T}$ and denote the effects of parametric uncertainties in task-space as

$$\tilde{\boldsymbol{B}}_\mathrm{p}\dot{\boldsymbol{x}}_2 + \tilde{\boldsymbol{d}}_\mathrm{pn} = -\boldsymbol{\varphi}_2^\mathrm{T}(\boldsymbol{x}_1, \boldsymbol{x}_2)\tilde{\boldsymbol{\beta}}_\mathrm{t} \tag{21}$$

where $\boldsymbol{\varphi}_2$ is a regressor given by $\boldsymbol{\varphi}_2 = [-\mathrm{diag}(\boldsymbol{G}^\mathrm{T}\boldsymbol{G}\dot{\boldsymbol{x}}_2), -\boldsymbol{E}_{3\times3}]^\mathrm{T}$ with $\boldsymbol{E}_{3\times3} = \mathrm{diag}([1, 1, 1]^\mathrm{T})$. The desired drive moment $\boldsymbol{\tau}_\mathrm{d}$ consists of two terms

$$\boldsymbol{\tau}_\mathrm{d} = \boldsymbol{\tau}_\mathrm{da} + \boldsymbol{\tau}_\mathrm{ds}, \qquad \boldsymbol{\tau}_\mathrm{da} = \boldsymbol{I}_\mathrm{p}(\ddot{\boldsymbol{y}}_\mathrm{d} - \boldsymbol{K}_\mathrm{c}\dot{\boldsymbol{z}}_1) - \boldsymbol{\varphi}_2^\mathrm{T}\hat{\boldsymbol{\beta}}_\mathrm{t} \tag{22}$$

where $\boldsymbol{\tau}_\mathrm{da}$ functions as the adaptive control part used to achieve an improved model compensation through on-line parameter adaptation via $\hat{\boldsymbol{\beta}}_\mathrm{t}$, and $\boldsymbol{\tau}_\mathrm{ds}$ is a robust control law to be synthesized later. $\hat{\boldsymbol{\beta}}_\mathrm{t}$ is updated by an adaptation law of the form Eq. (17), i.e.,

$$\dot{\hat{\boldsymbol{\beta}}}_\mathrm{t} = \mathrm{Proj}_{\hat{\boldsymbol{\beta}}}(\boldsymbol{\Gamma}_2\boldsymbol{\sigma}_2) \tag{23}$$

with the parameter adaptation function given by $\boldsymbol{\sigma}_2 = \boldsymbol{\varphi}_2\boldsymbol{I}_\mathrm{p}^{-\mathrm{T}}\boldsymbol{z}_2$. And $\boldsymbol{\tau}_\mathrm{ds}$ consists of two terms

$$\boldsymbol{\tau}_\mathrm{ds} = \boldsymbol{\tau}_\mathrm{ds1} + \boldsymbol{\tau}_\mathrm{ds2}, \qquad \boldsymbol{\tau}_\mathrm{ds1} = -\boldsymbol{I}_\mathrm{p}\boldsymbol{K}_2\boldsymbol{z}_2 \tag{24}$$

where $\boldsymbol{K}_2$ is a positive definite feedback gain matrix. $\boldsymbol{\tau}_\mathrm{ds2}$ is synthesized to dominate the model uncertainties coming from both parametric uncertainties and uncertain nonlinearities, which is chosen to satisfy the following conditions.

$$\begin{cases} \boldsymbol{z}_2^\mathrm{T}[\boldsymbol{I}_\mathrm{p}^{-1}(\boldsymbol{\tau}_\mathrm{ds2} - \boldsymbol{\varphi}_2^\mathrm{T}\tilde{\boldsymbol{\beta}}_\mathrm{p} - \tilde{\boldsymbol{d}}_\mathrm{p})] \le \varepsilon_2 \\ \boldsymbol{z}_2^\mathrm{T}\boldsymbol{I}_\mathrm{p}^{-1}\boldsymbol{\tau}_\mathrm{ds2} \le 0 \end{cases} \tag{25}$$

where ε_2 is a positive design parameter that can be arbitrarily small. How to choose $\boldsymbol{\tau}_\mathrm{ds2}$ to satisfy constraints like Eq. (25) can be found in Yao and Tomizuka (1997).

Denote the input discrepancy as $\boldsymbol{z}_3 = \boldsymbol{\tau} - \boldsymbol{\tau}_\mathrm{d}$. Differentiate Eq. (20) and substitute Eqs. (22) and (24) into it while noting Eq. (16), then

$$\dot{\boldsymbol{z}}_2 = -\boldsymbol{K}_2\boldsymbol{z}_2 + \boldsymbol{I}_\mathrm{p}^{-1}\boldsymbol{z}_3 + \boldsymbol{I}_\mathrm{p}^{-1}(\boldsymbol{\tau}_\mathrm{ds2} - \boldsymbol{\varphi}_2^\mathrm{T}\tilde{\boldsymbol{\beta}}_\mathrm{t} - \tilde{\boldsymbol{d}}_\mathrm{p}). \tag{26}$$

Define two positive semi-definite (p.s.d) functions $V_2 = \frac{1}{2}\boldsymbol{z}_2^\mathrm{T}\boldsymbol{z}_2$ for robust control and $V_{2a} = V_2 + \frac{1}{2}\tilde{\boldsymbol{\beta}}_\mathrm{t}^\mathrm{T}\boldsymbol{\Gamma}_2^{-1}\tilde{\boldsymbol{\beta}}_\mathrm{t}$ for adaptive control. From Eq. (26), the time derivative of V_2 is

$$\dot{V}_2 = -\boldsymbol{z}_2^\mathrm{T}\boldsymbol{K}_2\boldsymbol{z}_2 + \boldsymbol{z}_2^\mathrm{T}\boldsymbol{I}_\mathrm{p}^{-1}\boldsymbol{z}_3 + \boldsymbol{z}_2^\mathrm{T}\boldsymbol{I}_\mathrm{p}^{-1}(\boldsymbol{\tau}_\mathrm{ds2} - \boldsymbol{\varphi}_2^\mathrm{T}\tilde{\boldsymbol{\beta}}_\mathrm{t} - \tilde{\boldsymbol{d}}_\mathrm{p}). \tag{27}$$

And the time derivative of V_{2a} is

$$\begin{aligned} \dot{V}_{2a} = {} & -\boldsymbol{z}_2^\mathrm{T}\boldsymbol{K}_2\boldsymbol{z}_2 + \boldsymbol{z}_2^\mathrm{T}\boldsymbol{I}_\mathrm{p}^{-1}\boldsymbol{z}_3 + \boldsymbol{z}_2^\mathrm{T}\boldsymbol{I}_\mathrm{p}^{-1}(\boldsymbol{\tau}_\mathrm{ds2} - \tilde{\boldsymbol{d}}_\mathrm{p}) \\ & + \tilde{\boldsymbol{\beta}}_\mathrm{t}^\mathrm{T}(-\boldsymbol{\varphi}_2\boldsymbol{I}_\mathrm{p}^{-\mathrm{T}}\boldsymbol{z}_2 + \boldsymbol{\Gamma}_2^{-1}\dot{\tilde{\boldsymbol{\beta}}}_\mathrm{t}). \end{aligned} \tag{28}$$

When $\boldsymbol{z}_3 = 0$, substitute the first equation of Eq. (25) into Eq. (27), one obtains

$$\dot{V}_2 \le -\boldsymbol{z}_2^\mathrm{T}\boldsymbol{K}_2\boldsymbol{z}_2 + \varepsilon_2. \tag{29}$$

Thus, $\boldsymbol{z}_2$ will exponentially converge to the ball $\boldsymbol{z}_2 \le \sqrt{\varepsilon_2/\lambda_\mathrm{min}(\boldsymbol{K}_2)}$ and then be ultimately bounded. Furthermore, if the system is devoid of uncertain nonlinearities (i.e., $\tilde{\boldsymbol{d}}_\mathrm{p} = 0$), substitute Eq. (23) and the second equation of Eq. (25) into Eq. (28) while noting Eq. (19), one obtains

$$\dot{V}_{2a} \le -\boldsymbol{z}_2^\mathrm{T}\boldsymbol{K}_2\boldsymbol{z}_2. \tag{30}$$

Hence $\boldsymbol{z}_2$ will asymptotically converge to zero and an improved steady-state tracking performance will be obtained.

(2) Step 2

The next step is to synthesize the air mass flow rate $\boldsymbol{q}_\mathrm{m}$ so that $\boldsymbol{z}_3$ converges to a small value or zero with a guaranteed transient performance. For this purpose, first note that the unknown parameter vector in muscle-space is $\boldsymbol{\beta}_\mathrm{m} = [\lambda_{a1}, \lambda_{a2}, \lambda_{a3}, \lambda_{b1}, \lambda_{b2}, \lambda_{b3}, d_{\tau\mathrm{n}1}, d_{\tau\mathrm{n}2}, d_{\tau\mathrm{n}3}]^\mathrm{T}$. Then the terms due to parametric uncertainties in muscle-space can be described by

$$\tilde{\boldsymbol{f}}_\tau + \tilde{\boldsymbol{g}}_\tau\boldsymbol{q}_\mathrm{m} + \tilde{\boldsymbol{d}}_{\tau\mathrm{n}} = \boldsymbol{\varphi}_3^\mathrm{T}\tilde{\boldsymbol{\beta}}_\mathrm{m} \tag{31}$$

where $\boldsymbol{\varphi}_3 = [-\boldsymbol{J}_\theta^\mathrm{T}\frac{\partial\bar{\boldsymbol{F}}_\mathrm{m}}{\partial\boldsymbol{p}}\boldsymbol{A}_f, \boldsymbol{J}_\theta^\mathrm{T}\frac{\partial\bar{\boldsymbol{F}}_\mathrm{m}}{\partial\boldsymbol{p}}\boldsymbol{A}_\mathrm{g}\mathrm{diag}(\boldsymbol{K}_\mathrm{q}\boldsymbol{u}), \boldsymbol{E}_{3\times3}]^\mathrm{T}$ is the regressor for parameter adaptation, $\hat{\boldsymbol{\beta}}_\mathrm{m}$ is updated by an adaptation law of the form Eq. (17), i.e.,

$$\dot{\hat{\boldsymbol{\beta}}}_\mathrm{m} = \mathrm{Proj}_{\hat{\boldsymbol{\beta}}}(\boldsymbol{\Gamma}_3\boldsymbol{\sigma}_3) \tag{32}$$

with the parameter adaptation function given by $\boldsymbol{\sigma}_3 = \boldsymbol{\varphi}_3\boldsymbol{z}_3$.

From Eqs. (15) and (22), the dynamics of $\boldsymbol{z}_3$ is

$$\dot{\boldsymbol{z}}_3 = \dot{\boldsymbol{\tau}} - \dot{\boldsymbol{\tau}}_\mathrm{d} = \boldsymbol{f}_\tau + \boldsymbol{g}_\tau\boldsymbol{q}_\mathrm{m} + \boldsymbol{d}_\tau - \dot{\boldsymbol{\tau}}_\mathrm{dc} - \dot{\boldsymbol{\tau}}_\mathrm{du} \tag{33}$$

where $\dot{\boldsymbol{\tau}}_\mathrm{dc} = \frac{\partial\boldsymbol{\tau}_\mathrm{d}}{\partial t} + \frac{\partial\boldsymbol{\tau}_\mathrm{d}}{\partial\boldsymbol{x}_1}\hat{\boldsymbol{x}}_2 + \frac{\partial\boldsymbol{\tau}_\mathrm{d}}{\partial\boldsymbol{x}_2}\dot{\hat{\boldsymbol{x}}}_2 + \frac{\partial\boldsymbol{\tau}_\mathrm{d}}{\partial\hat{\boldsymbol{\beta}}_\mathrm{t}}\dot{\hat{\boldsymbol{\beta}}}_\mathrm{t}$, $\dot{\boldsymbol{\tau}}_\mathrm{du} = \frac{\partial\boldsymbol{\tau}_\mathrm{d}}{\partial\boldsymbol{x}_1}(\boldsymbol{x}_2 - \hat{\boldsymbol{x}}_2) + \frac{\partial\boldsymbol{\tau}_\mathrm{d}}{\partial\boldsymbol{x}_2}(\dot{\boldsymbol{x}}_2 - \dot{\hat{\boldsymbol{x}}}_2)$ in which $\hat{\boldsymbol{x}}_2$ and $\dot{\hat{\boldsymbol{x}}}_2$ are estimates of $\boldsymbol{x}_2$ and $\dot{\boldsymbol{x}}_2$ respectively, and are deduced from $\boldsymbol{x}_1$ by an output differential observer. Note that $\dot{\boldsymbol{\tau}}_\mathrm{dc}$ represents the calculable part of $\dot{\boldsymbol{\tau}}_\mathrm{d}$ and can be used to design control input $\boldsymbol{u}$, but $\dot{\boldsymbol{\tau}}_\mathrm{du}$ cannot, due to various uncertainties. The desired mass flow rate is

$$\begin{aligned} & \boldsymbol{q}_\mathrm{md} = \boldsymbol{q}_\mathrm{mda} + \boldsymbol{q}_\mathrm{mds}, \\ & \boldsymbol{q}_\mathrm{mda} = \hat{\boldsymbol{g}}_\tau^{-1}(-\boldsymbol{I}_\mathrm{p}^{-\mathrm{T}}\boldsymbol{z}_2 - \hat{\boldsymbol{f}}_\tau - \hat{\boldsymbol{d}}_{\tau\mathrm{n}} + \dot{\boldsymbol{\tau}}_\mathrm{dc}) \end{aligned} \tag{34}$$

where $\boldsymbol{q}_\mathrm{mda}$ is used for adaptive model compensation and the robust control law $\boldsymbol{q}_\mathrm{mds}$ consists of the following two terms.

$$\boldsymbol{q}_\mathrm{mds} = \boldsymbol{q}_\mathrm{mds1} + \boldsymbol{q}_\mathrm{mds2}, \qquad \boldsymbol{q}_\mathrm{mds1} = -\hat{\boldsymbol{g}}_\tau^{-1}\boldsymbol{K}_3\boldsymbol{z}_3 \tag{35}$$

where $\boldsymbol{K}_3$ is a positive definite feedback gain matrix and $\boldsymbol{q}_\mathrm{mds2}$ is a nonlinear robust feedback function chosen to satisfy the following conditions for dominating all model uncertainties.

$$\begin{cases} \boldsymbol{z}_3^\mathrm{T}[\hat{\boldsymbol{g}}_\tau\boldsymbol{q}_\mathrm{mds2} - \boldsymbol{\varphi}_3^\mathrm{T}\tilde{\boldsymbol{\beta}}_\mathrm{m} + \tilde{\boldsymbol{d}}_3] \le \varepsilon_3 \\ \boldsymbol{z}_3^\mathrm{T}\hat{\boldsymbol{g}}_\tau\boldsymbol{q}_\mathrm{mds2} \le 0 \end{cases} \tag{36}$$

where $\boldsymbol{d}_3 = \tilde{\boldsymbol{d}}_\tau - \dot{\boldsymbol{\tau}}_\mathrm{du}$ represents the total uncertainties in muscle-space, ε_3 is a positive design parameter. How to choose $\boldsymbol{q}_\mathrm{mds2}$ to satisfy constraints like Eq. (36) can also be found in Yao and Tomizuka (1997).

Define two p.s.d. functions $V_3 = V_2 + \frac{1}{2}\boldsymbol{z}_3^\mathrm{T}\boldsymbol{z}_3$ for robust control and $V_{3a} = V_{2a} + \frac{1}{2}\tilde{\boldsymbol{\beta}}_\mathrm{m}^\mathrm{T}\boldsymbol{\Gamma}_3^{-1}\tilde{\boldsymbol{\beta}}_\mathrm{m}$ for adaptive control. While noting Eqs. (33)–(35), the time derivative of V_3 is

$$\begin{aligned} \dot{V}_3 = {} & -\boldsymbol{z}_2^\mathrm{T}\boldsymbol{K}_2\boldsymbol{z}_2 + \boldsymbol{z}_2^\mathrm{T}\boldsymbol{I}_\mathrm{p}^{-1}(\boldsymbol{\tau}_\mathrm{ds2} - \boldsymbol{\varphi}_2^\mathrm{T}\tilde{\boldsymbol{\beta}}_\mathrm{t} - \tilde{\boldsymbol{d}}_\mathrm{p}) \\ & - \boldsymbol{z}_3^\mathrm{T}\boldsymbol{K}_3\boldsymbol{z}_3 + \boldsymbol{z}_3^\mathrm{T}(\hat{\boldsymbol{g}}_\tau\boldsymbol{q}_\mathrm{mds2} - \boldsymbol{\varphi}_3^\mathrm{T}\tilde{\boldsymbol{\beta}}_\mathrm{m} + \tilde{\boldsymbol{d}}_3). \end{aligned} \tag{37}$$

The time derivative of V_{3a} is

$$\begin{aligned} \dot{V}_{3a} = {} & -\boldsymbol{z}_2^\mathrm{T}\boldsymbol{K}_2\boldsymbol{z}_2 + \boldsymbol{z}_2^\mathrm{T}\boldsymbol{I}_\mathrm{p}^{-1}(\boldsymbol{\tau}_\mathrm{ds2} - \tilde{\boldsymbol{d}}_\mathrm{p}) \\ & + \tilde{\boldsymbol{\beta}}_\mathrm{t}^\mathrm{T}(-\boldsymbol{\varphi}_2\boldsymbol{I}_\mathrm{p}^{-\mathrm{T}}\boldsymbol{z}_2 + \boldsymbol{\Gamma}_2^{-1}\dot{\tilde{\boldsymbol{\beta}}}_\mathrm{t}) - \boldsymbol{z}_3^\mathrm{T}\boldsymbol{K}_3\boldsymbol{z}_3 \\ & + \boldsymbol{z}_3^\mathrm{T}(\hat{\boldsymbol{g}}_\tau\boldsymbol{q}_\mathrm{mds2} + \tilde{\boldsymbol{d}}_3) + \tilde{\boldsymbol{\beta}}_\mathrm{m}^\mathrm{T}(-\boldsymbol{\varphi}_3\boldsymbol{z}_3 + \boldsymbol{\Gamma}_3^{-1}\dot{\tilde{\boldsymbol{\beta}}}_\mathrm{m}). \end{aligned} \tag{38}$$

Substituting the first equation of Eq. (25) and the first equation of Eq. (36) into Eq. (37), one obtains

$$\dot{V}_3 \le -\boldsymbol{z}_2^\mathrm{T}\boldsymbol{K}_2\boldsymbol{z}_2 - \boldsymbol{z}_3^\mathrm{T}\boldsymbol{K}_3\boldsymbol{z}_3 + \varepsilon_2 + \varepsilon_3. \tag{39}$$

Thus, $\boldsymbol{z}_2$ and $\boldsymbol{z}_3$ will exponentially converge to some balls whose sizes are proportional to ε_2 and ε_3, and thus be ultimately bounded. Furthermore, if the system is devoid of uncertain nonlinearities

(i.e., $\tilde{\boldsymbol{d}}_{\mathrm{p}} = 0$ and $\tilde{\boldsymbol{d}}_3 = 0$), substitute Eqs. (23), (32), the second equation of Eq. (25) and the second equation of Eq. (36) into Eq. (38) while noting Eq. (19), one obtains

$$\dot{V}_{3a} \leq -\boldsymbol{z}_2^{\mathrm{T}}\boldsymbol{K}_2\boldsymbol{z}_2 - \boldsymbol{z}_3^{\mathrm{T}}\boldsymbol{K}_3\boldsymbol{z}_3. \tag{40}$$

Hence asymptotic output tracking (or zero final tracking error) is obtained as well.

(3) Step 3

The inverse flow rate mapping is used to calculate the specific duty cycle commands of the fast switching valves for providing the desired flow rate $\boldsymbol{q}_{\mathrm{md}}$. The control input vector is

$$\boldsymbol{u} = \boldsymbol{K}_{\mathrm{q}}^{-1}(\boldsymbol{p}, \mathrm{sign}(\boldsymbol{q}_{\mathrm{md}}))\boldsymbol{q}_{\mathrm{md}}. \tag{41}$$

3.4. Output differential observer

In the above controller development, the velocity and acceleration of the PMDPM are needed in the calculation of Eq. (34). To obtain these signals based on the posture only, an output differential observer is developed as follows. After the actual contractive lengths of pneumatic muscles are measured, kinematics solution is employed to get the posture of the PMDPM. And then an output differential observer given by Eq. (42) is used to estimate the corresponding velocity and acceleration of the PMDPM (Qi, Chen, & Yuan, 2003).

$$\begin{cases} \dot{\hat{x}}_{i1} = \hat{x}_{i2} + a_1(\theta_i - \hat{x}_{i1}) \\ \dot{\hat{x}}_{i2} = \hat{x}_{i3} + a_2(\theta_i - \hat{x}_{i1}) \\ \dot{\hat{x}}_{i3} = a_3(\theta_i - \hat{x}_{i1}) \end{cases} \tag{42}$$

where $\hat{x}_{i1} = \hat{\theta}_i$, $\hat{x}_{i2} = \dot{\hat{\theta}}_i$ and $\hat{x}_{i2} = \ddot{\hat{\theta}}_i$ with i representing x, y and z axes respectively.

The transfer function of the above observer is

$$\frac{\hat{x}_{i1}(s)}{\theta_i(s)} = \frac{a_1 s^2 + a_2 s + a_3}{s^3 + a_1 s^2 + a_2 s + a_3}. \tag{43}$$

Pole-placement method is utilized to specify the values of a_1, a_2, a_3 according to the desired closed-loop bandwidth. The error of output differential observer can be lumped into uncertain nonlinearities $\tilde{\boldsymbol{d}}_{\mathrm{p}}$ and $\tilde{\boldsymbol{d}}_{\tau}$, which can be attenuated by robust control.

3.5. Analysis of design parameters

In the above design procedure, $\boldsymbol{K}_{\mathrm{c}}$, $\boldsymbol{K}_2$, $\boldsymbol{K}_3$, ε_2, ε_3 and adaptation rates $\boldsymbol{\Gamma}_2$ and $\boldsymbol{\Gamma}_3$ are the design parameters. Their values have significant effect on transient performance and final tracking errors, and can be qualitatively analyzed as follows.

(a) $\boldsymbol{K}_{\mathrm{c}}$ affects the speed of $\boldsymbol{z}_1$ converging to zero. A larger magnitude of $\boldsymbol{K}_{\mathrm{c}}$ contributes to the higher speed of $\boldsymbol{z}_1$ converging to zero while it is constrained by the bandwidth of the total control system due to unmodeled high frequency dynamics, saturation of control input, sampling frequency of digital implementation, etc. In conclusion, the magnitude of $\boldsymbol{K}_{\mathrm{c}}$ should be set as large as possible under the circumstance of no vibrations observed in the controlled system.

(b) $\boldsymbol{K}_2$, $\boldsymbol{K}_3$, ε_2 and ε_3 contribute to the control accuracy and transient performance as follows. The solution of Eq. (39) satisfies

$$V_3(t) \leq \exp(-\lambda_v t)V_3(0) + \frac{\varepsilon_v}{\lambda_v}[1 - \exp(-\lambda_v t)] \tag{44}$$

where $\lambda_v = 2 \times \min\{\sigma_{\min}(\boldsymbol{K}_2), \sigma_{\min}(\boldsymbol{K}_3)\}$ in which $\sigma_{\min}(\bullet)$ denotes the minimum eigenvalue of a matrix, and $\varepsilon_v = \varepsilon_2 + \varepsilon_3$. As can be seen from Eq. (44), smaller magnitudes of ε_2 and ε_3 and larger magnitudes of $\boldsymbol{K}_2$ and $\boldsymbol{K}_3$ should be chosen for faster converging rate and smaller steady-state values of tracking errors. However, they are also constrained by the achievable bandwidth of a closed-loop system like $\boldsymbol{K}_{\mathrm{c}}$.

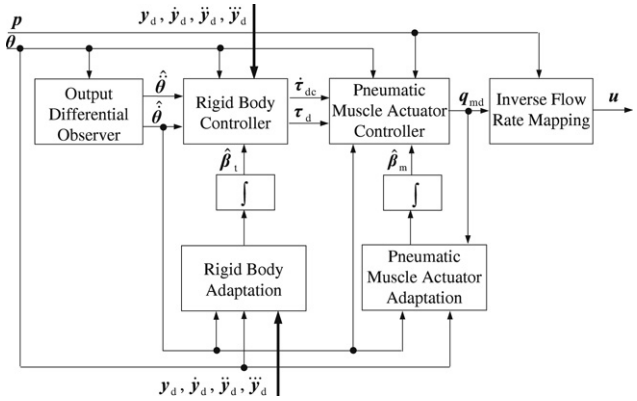

Fig. 2. Proposed control strategy of the PMDPM.

3.6. Desired trajectory generation

In implementation, the desired trajectory should be initialized and generated appropriately for a guaranteed transient performance (Yao & Tomizuka, 1997). The desired trajectory $\boldsymbol{y}_{\mathrm{d}}$ and its derivatives $\dot{\boldsymbol{y}}_{\mathrm{d}}$, $\ddot{\boldsymbol{y}}_{\mathrm{d}}$, $\dddot{\boldsymbol{y}}_{\mathrm{d}}$ are generated from the actual reference trajectory through a third-order stable filter given by Eq. (45)

$$\dddot{\boldsymbol{y}}_{\mathrm{d}} + \kappa_1\ddot{\boldsymbol{y}}_{\mathrm{d}} + \kappa_2\dot{\boldsymbol{y}}_{\mathrm{d}} + \kappa_3\boldsymbol{y}_{\mathrm{d}} = \dddot{\boldsymbol{y}}_{\mathrm{r}} + \kappa_1\ddot{\boldsymbol{y}}_{\mathrm{r}} + \kappa_2\dot{\boldsymbol{y}}_{\mathrm{r}} + \kappa_3\boldsymbol{y}_{\mathrm{r}} \tag{45}$$

where κ_1, κ_2, κ_3 are design parameters of the filter with initialization.

Putting all the above developments together, the proposed control strategy of the PMDPM is schematically represented in Fig. 2.

4. Simulation results

For the PMDPM, two controllers, the proposed adaptive robust controller (ARC) and a deterministic robust controller (DRC), are first compared through simulation results. The ARC utilizes parameter adaptation to estimate lumped disturbances and other unknown parameters as detailed in the previous section, whereas the DRC has the same control law as the ARC but without using parameter adaptation. The system parameters in simulation are selected based upon their actual values of the experimental setup that will be detailed in the next section and are given in Table 1. The control algorithms and the plant dynamics are all implemented using Matlab Simulink™ toolbox. The estimated parameters of the controllers are initially set to values different from those used in the plant models to investigate the ability of the controllers to cope with parametric uncertainties. The friction force model of pneumatic muscle used in plant dynamics is described by Eq. (46) to investigate the effectiveness of the controllers in compensating large unknown nonlinearities (Tondu & Lopez, 2000).

$$F_{\mathrm{f}i} = f_{\mathrm{s}} S_{ei} p_i \mathrm{sign}(\dot{x}_{\mathrm{m}i}) \tag{46}$$

where $S_{\mathrm{e}i} = \pi D_0 L_0 \frac{\sin\alpha_0}{(1-\varepsilon_{\mathrm{m}i})\sqrt{1-\cos^2\alpha_0(1-\varepsilon_{\mathrm{m}i})^2}}$ and f_{s} is the friction coefficient.

In the following simulations and experiments, the rotational angle θ_z of the posture vector is not controlled, as it is normally very small for the PMDPM studied in this paper and not important in practice. The control algorithms implemented are obtained by setting $\theta_z = \theta_{\mathrm{zd}} = 0$ in previous sections. The simulation results of tracking a smooth square trajectory are shown in Fig. 3. The results indicate that the ARC performs much better than the DRC for this system due to the quite large extent of parametric uncertainties and disturbances in the system. The DRC cannot handle such large disturbances that large tracking errors come into existence.

Table 1
Parameters in simulation

Parameters	Quantity	Parameters	Quantity
D_0 (m)	0.04	$\boldsymbol{I}([I_x, I_y, I_z])$ (kg m^2)	[0.457, 0.457, 0.864]
δ_0 (m)	0.004	$\boldsymbol{M}([m_1, m_2, m_3])$ (kg)	[2, 2, 2]
E (MPa)	10	$\boldsymbol{C}_s([c_{s1}, c_{s2}, c_{s3}])$ (N m s/rad)	[10, 10, 10]
a (m^2)	0.0203	$\bar{\boldsymbol{\delta}}(t)([\bar{\delta}_x, \bar{\delta}_y, \bar{\delta}_z])$ (N m)	[−20, 30, 0]
b (m^2)	0.0083	$\boldsymbol{\lambda}_a([\lambda_{a1}, \lambda_{a2}, \lambda_{a3}])$	[1.3, 1.3, 1.3]
P_s (MPa)	0.48	$\boldsymbol{\lambda}_b([\lambda_{b1}, \lambda_{b2}, \lambda_{b3}])$	[1.3, 1.3, 1.3]
T_s (K)	300	$\boldsymbol{d}_\tau([d_{\tau1}, d_{\tau2}, d_{\tau3}])$ (N m/s)	[0, 0, 0]
L_0 (m)	0.6	f_S	0.042
α_0(°)	25.339		

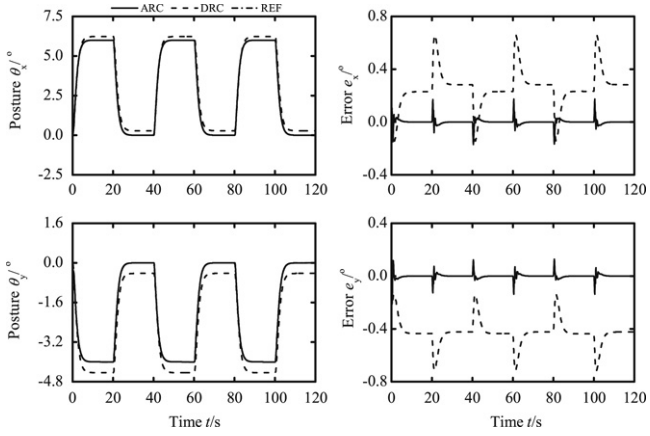

Fig. 3. Smooth square trajectory motion in simulation.

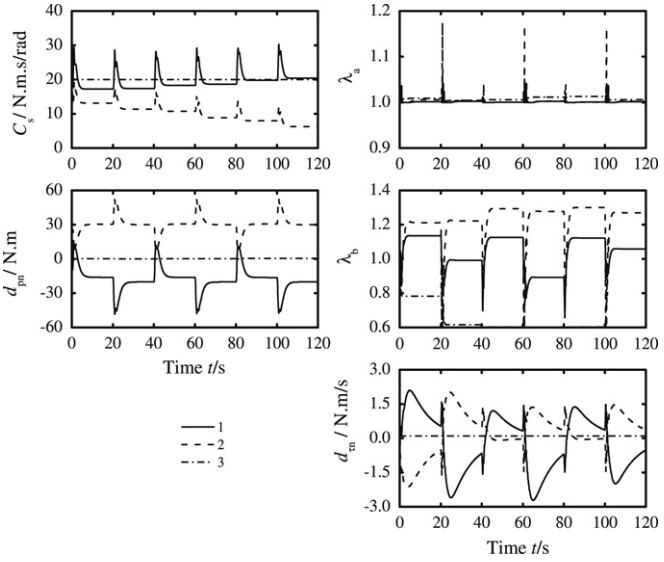

Fig. 4. Estimated parameters in simulation. Note: 1, 2, 3 represent estimated parameters of three driving units or three axes respectively.

Though increasing $\boldsymbol{K}_c$ can decrease the final tracking errors, it also causes much control input chattering due to noise, as analyzed in Section 3. In contrast, lumped disturbance estimates in the ARC compensate for various uncertainties in task-space well and very small tracking errors are seen at the steady-state, though parameter estimates of the ARC in Fig. 4 may not converge to their true values.

5. Experimental results

5.1. Experiment setup

The schematic diagram of the PMDPM system shown in Fig. 5 is used to evaluate the effectiveness of the proposed controller.

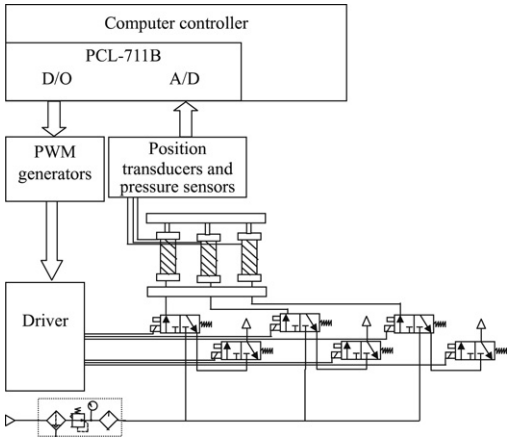

Fig. 5. Schematic diagram of the PMDPM system.

Fig. 6. Picture of the PMDPM system.

Fig. 6 is the picture of the PMDPM system. Three pneumatic muscles used in experiments are Fluidic Muscles manufactured by Festo (MAS-40-N600-AA-MCKK). Two fast switching valves are used to regulate the pressure inside each pneumatic muscle. A data acquisition card is used to receive signals from two position transducers by D/A and to send out PWM signals by D/O for driving six fast switching valves (MHE2-MS1H-3/2G-M7-K). Position transducers and pressure sensors are used to measure contractive lengths and inner pressures of pneumatic muscles respectively. Industrial computer is used as a controller for processing signals and outputting control commands.

5.2. Comparative experiments

The effectiveness of the proposed controller has been demonstrated by a number of experiments under the supply pressure of 0.48 MPa. Some typical results are given below.

(1) Smooth step response

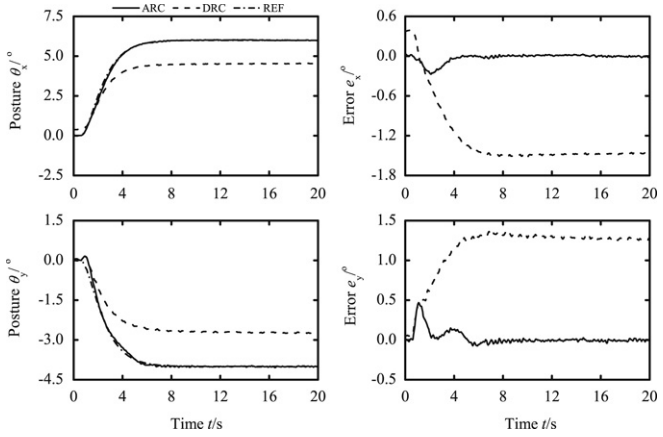

Fig. 7. Smooth step response with a rise time of 5 s.

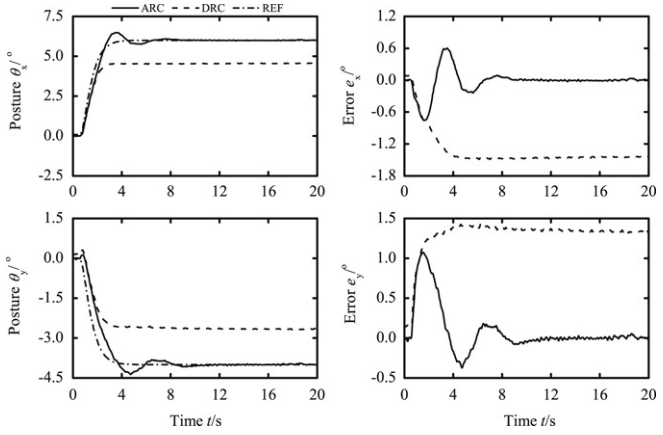

Fig. 8. Smooth step response with a rise time of 2.5 s.

The two controllers (ARC and DRC) are first tested by a slow smooth step response with a rise time of 5 s as shown in Fig. 7, where the posture is from $\theta_x = 0°$, $\theta_y = 0°$ to $\theta_x = 6°$, $\theta_y = -4°$. As can be seen from Fig. 7, the ARC performs much better than the DRC: final errors of the ARC are $e_{xF} = 0.0195°$ and $e_{yF} = 0.0232°$ and maximal absolute errors during the entire run are $e_{xM} = 0.2694°$ and $e_{yM} = 0.4685°$.

The two controllers are then run for a fast smooth step response with a rise time of 2.5 s as shown in Fig. 8. And the estimated lumped uncertainties are shown in Fig. 9. Due to the saturated control inputs shown in Fig. 10, there are slightly large tracking errors in both x-axis and y-axis under the control of ARC. Nevertheless steady-state errors are almost the same as those of the slow smooth step response in Fig. 7. This indicates that it is necessary to design reference motion trajectories taking into account the effect of control input saturation level as well.

To test the robustness of the proposed controller to sudden disturbances, one position transducer is given a sudden dither, which can be regarded as a sudden large output disturbance of the system. The responses of this situation are shown in Fig. 11. As can be seen, the system experiences large tracking errors due to the wrong feedback information of the position transducer when the dither is introduced. But after the dither disappears, the system comes back to the stable posture quickly. This verifies the robustness of the proposed controller to disturbances.

(2) Smooth square trajectory motion

The response of tracking the same smooth square trajectory as in the simulation is shown in Fig. 12. Comparing Fig. 3 with Fig. 12, responses of the ARC are similar while the responses of the DRC are significantly different. It is caused by different

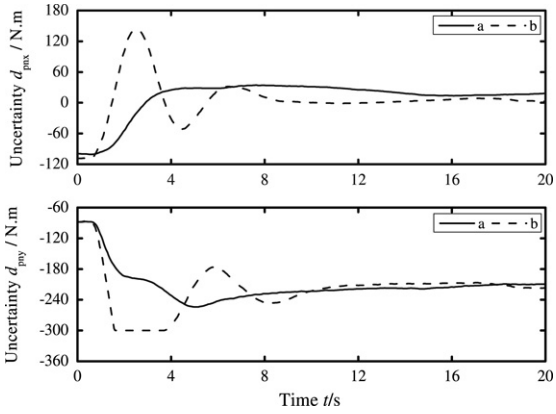

Fig. 9. Estimated lumped uncertainties of slow and fast smooth step responses. Note: (a) and (b) represent slow and fast smooth step responses respectively.

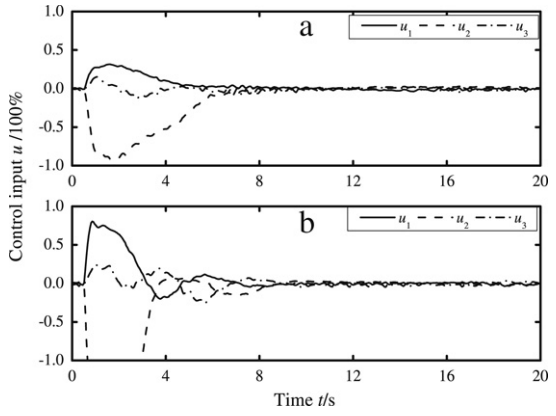

Fig. 10. Control inputs of the ARC for fast and slow smooth step responses.

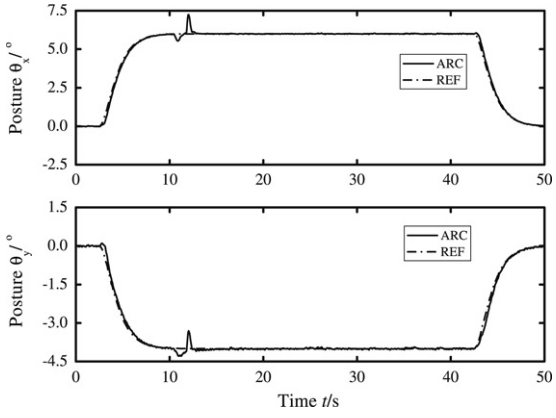

Fig. 11. Robustness to a sudden disturbance.

static forces of pneumatic muscles $\boldsymbol{F}_{\mathrm{m}}$, different friction forces of pneumatic muscles $\boldsymbol{F}_{\mathrm{f}}$ and different external disturbances $\tilde{\boldsymbol{\delta}}(t)$ between simulation and experiment. Tracking errors of the DRC cannot be small enough since not only there are large modeling errors of $\boldsymbol{F}_{\mathrm{m}}$, $\boldsymbol{F}_{\mathrm{f}}$ and $\tilde{\boldsymbol{\delta}}(t)$, but also design parameters such as $\boldsymbol{K}_{\mathrm{c}}$, $\boldsymbol{K}_2$ cannot be large enough due to the neglected high frequency dynamics. In contrast, the ARC can effectively compensate for large modeling errors through parameter adaptation as shown in Fig. 13 and thus obtain very small final tracking errors in steady-state ($\tilde{\boldsymbol{d}}_{\mathrm{p}} = 0$ and $\tilde{\boldsymbol{d}}_{\tau} = 0$).

(3) Sinusoidal trajectory motion

The two controllers are also run for tracking sinusoidal trajectories with different frequencies. For example, Fig. 14 shows

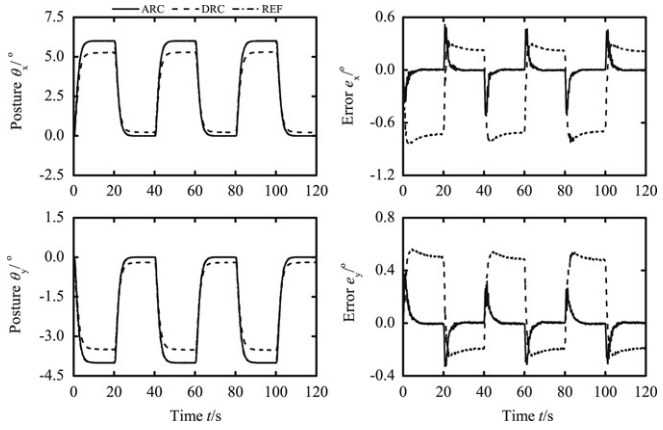

Fig. 12. Smooth square trajectory motion.

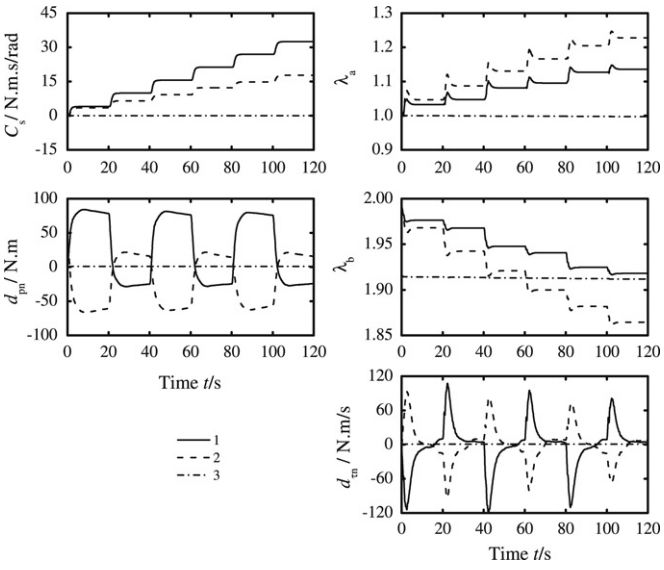

Fig. 13. Estimated parameters of smooth square trajectory motion.

a sinusoidal trajectory motion with a period of 20 s and an amplitude of $\theta_x = 6°$, $\theta_y = 4°$. And Fig. 15 plots estimated lumped uncertainties in task-space. Similarly, Fig. 16 is a sinusoidal trajectory motion with a period of 15 s. It is confirmed once more that the ARC achieves much better performance than the DRC. For tracking a sinusoidal trajectory with the period of 20 s, average errors of the ARC in terms of L_2 norm are $L_2[e_x] = 0.1299°$ and $L_2[e_y] = 0.1012°$ and the maximal absolute errors are $e_{xM} = 0.3688°$ and $e_{yM} = 0.3033°$.

6. Conclusions

The posture trajectory tracking of a parallel manipulator driven by pneumatic muscles has been investigated in the paper. There are not only time-varying friction forces and static force model errors in the mathematical models of pneumatic muscles, but there are also strong coupling, inherent complex nonlinearities and unknown disturbances in the mathematical models of the parallel manipulator itself. For precise posture trajectory tracking of the PMDPM, an adaptive robust control strategy has been proposed to effectively handle these parametric uncertainties and uncertain nonlinearities considered in mathematical models of the plant. As proved by simulation and experimental results, the proposed controller achieves a guaranteed transient performance as well as a guaranteed final tracking accuracy. Moreover, zero final tracking errors could be achieved in the presence of parametric uncertainties only. In addition, an output differential observer is constructed for providing a simple and effective way to implement the proposed adaptive robust controller.

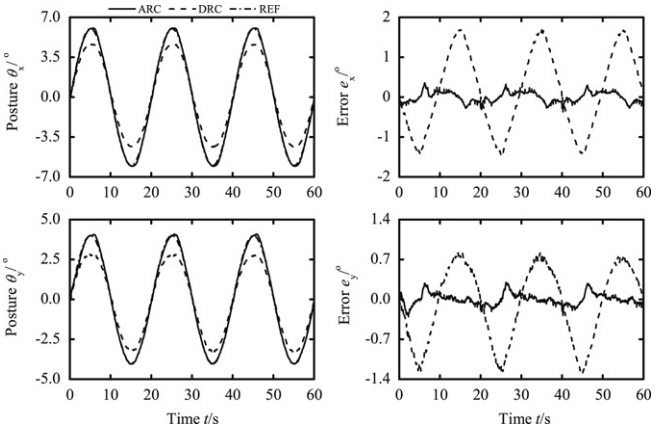

Fig. 14. Sinusoidal trajectory motion (period = 20 s).

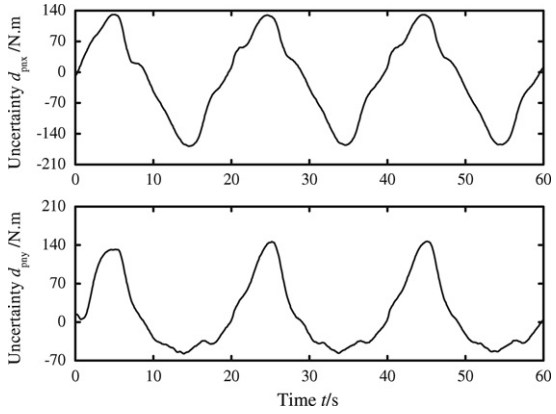

Fig. 15. Estimated lumped uncertainties of sinusoidal trajectory motion.

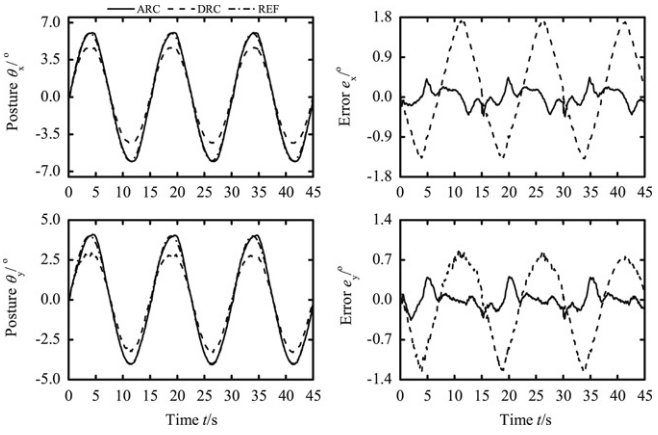

Fig. 16. Sinusoidal trajectory motion (period = 15 s).

Acknowledgements

The third author is supported by the National Natural Science Foundation of China (NSFC) under the Joint Research Fund (grant 50528505) for Overseas Chinese Young Scholars and a Kuang-piu Professorship at Zhejiang University.

References

Ahn, K. K., Thanh, T. D. C., & Yang, S. Y. (2004). Improvement of control performance of pneumatic artificial muscle manipulator using intelligent switching control. In *2004 SICE annual conference* (pp. 1593–1598).

Bowler, C. J., Caldwell, D. G., & Medrano-Cerda, G. A. (1996). Pneumatic muscle actuators: Musculature for an anthropomorphic robot arm. In *IEEE colloquium on actuator technology: current practice and new developments* (pp. 8/1–8/6).

Cai, D., & Yamaura, H. (1996). A robust controller for manipulator driven by artificial muscle actuator. In *Proceedings of the 1996 IEEE international conference on control applications* (pp. 540–545).

Carbonell, P., Jiang, Z. P., & Repperger, D. W. (2001). A fuzzy backstepping controller for a pneumatic muscle actuator system. In *Proceedings of the 2001 IEEE international symposium on intelligent control* (pp. 353–358).

Chan, S. W., Lilly, J. H., Repperger, D. W., & Berlin, J. E. (2003). Fuzzy PD+I learning control for a pneumatic muscle. In *IEEE international conference on fuzzy systems* (pp. 278–283).

Chou, C. P., & Hannaford, B. (1996). Measurement and modeling of McKibben pneumatic artificial muscles. *IEEE Transactions on Robotics and Automation*, *12*(1), 90–102.

Hildebrandt, A., Sawodny, O., Neumann, R., & Hartmann, A. (2002). A flatness based design for tracking control of pneumatic muscle actuators. In *The 7th international conference on control, automation, robotics and vision* (pp. 1156–1161).

Hildebrandt, A., Sawodny, O., Neumann, R., & Hartmann, A. (2005). Cascaded control concept of a robot with two degrees of freedom driven by four artificial pneumatic muscle actuators. In *American control conference* (pp. 680–685).

Huang, Z., Kou, L., & Fang, Y. (1997). *Theory of parallel robotic mechanisms and control*. Beijing: China Mechanical Press (in Chinese).

Kimoto, M., & Ito, H. (2003). Nonlinear robust compensation for control of a pneumatic actuator. In *SICE annual conference* (pp. 1820–1825).

Kimura, T., Hara, S., Fujita, T., & Kagawa, T. (1997). Feedback linearization for pneumatic actuators systems with static friction. *Control Engineering Practice*, *5*(10), 1385–1394.

Lilly, J. H. (2003). Adaptive tracking for pneumatic muscle actuators in bicep and tricep configurations. *IEEE Transactions on Neural Systems and Rehabilitation Engineering*, *11*(3), 333–339.

Lilly, J. H., & Quesada, P. M. (2004). A two-input sliding-mode controller for a planar arm actuated by four pneumatic muscle groups. *IEEE Transactions on Neural Systems and Rehabilitation Engineering*, *12*(3), 349–359.

Lilly, J. H., & Yang, L. (2005). Sliding mode tracking for pneumatic muscles actuators in opposing pair configuration. *IEEE Transactions on Control Systems Technology*, *13*(4), 550–558.

Qi, G. Y., Chen, Z. Q., & Yuan, Z. Z. (2003). High order differential feedback control for nonlinear systems. *Engineering Science*, *5*(8), 35–44 (in Chinese).

Repperger, D. W., Johnson, K. R., & Phillips, C. A. (1998). A VSC position tracking systems involving a large scale pneumatic muscle actuator. In *Proceedings of the 37th IEEE conference on decision & control* (pp. 4302–4307).

Repperger, D. W., Phillips, C. A., & Krier, M. (1999). Controller design involving gain scheduling for a large scale pneumatic muscle actuator. In *Proceedings of the 1999 IEEE international conference on control applications* (pp. 285–290).

Richer, E., & Hurmuzlu, Y. (2000). A high performance pneumatic force actuator system: Part I-nonlinear mathematical model. *Transactions of the ASME Journal of Dynamic Systems, Measurement, and Control*, *122*(3), 416–425.

Tao, G. L., Zhu, X. C., & Cao, J. (2005). Modeling and controlling of parallel manipulator joint driven by pneumatic muscles. *Chinese Journal of Mechanical Engineering(English Edition)*, *18*(4), 537–541.

Tian, S. P., Ding, G. Q., Yang, D. T., & Lin, L. M. (2004). Nonlinear modeling and controlling of artificial muscle system using neural networks. *Chinese Journal of Mechanical Engineering(English Edition)*, *17*(2), 306–310.

Tondu, B., & Lopez, P. (2000). Modeling and control of McKibben artificial muscle robot actuators. *IEEE Control Systems Magazine*, *20*(2), 15–38.

Xu, L., & Yao, B. (2001). Adaptive robust precision motion control of linear motors with negligible electrical dynamics: theory and experiments. *IEEE/ASME Transactions on Mechatronics*, *6*(4), 444–452.

Yang, G., Li, B. R., & Liu, J. (2002). A new analytical method on characteristics of artificial pneumatic muscle actuator. *Chinese Hydraulics and Pneumatics*, 22–25 (in Chinese).

Yao, B. (2003). Integrated direct/indirect adaptive robust control of SISO nonlinear systems in semi-strict feedback form. In *American control conference* (pp. 3020–3025).

Yao, B., Bu, F. P., Reedy, J., & Chiu, G. T. C. (2000). Adaptive robust motion control of single-rod hydraulic actuators: theory and experiments. *IEEE/ASME Transactions on Mechatronics*, *5*(1), 79–91.

Yao, B., & Tomizuka, M. (1997). Adaptive robust control of SISO nonlinear systems in a semi-strict feedback form. *Automatica*, *33*(5), 893–900.

Yao, B., & Tomizuka, M. (2001). Adaptive robust control of MIMO nonlinear systems in semi-strict feedback forms. *Automatica*, *37*(9), 1305–1321.

Xiaocong Zhu received the Ph.D. degree and B.Eng. degree in mechanical engineering from the Zhejiang University, Hangzhou, China, in 2007 and 2002, respectively.

She is currently a Postdoctor in the State Key Laboratory of Fluid Power Transmission and Control, Zhejiang University, Hangzhou, China. Her research interests include pneumatic servo control, nonlinear control theory and applications, mechatronic control, etc.

Guoliang Tao received the Ph.D. degree, M.Eng. degree and B.Eng. degree in mechanical engineering from the Zhejiang University, Hangzhou, China, in 2000, 1991 and 1985, respectively.

Since 1991, he has been with the State Key Laboratory of Fluid Power Transmission and Control, Zhejiang University, Hangzhou, China and was promoted to an Associate Researcher in 1997 and a Professor in 2001. His research interests include nonlinear control theory and applications, mechatronic control, fluid power transmission and control, especially pneumatic servo control and novel pneumatic components.

Bin Yao received the Ph.D. degree in mechanical engineering from the University of California, Berkeley, in 1996, the M.Eng. degree in electrical engineering from the Nanyang Technological University, Singapore, in 1992, and the B.Eng. degree in applied mechanics from the Beijing University of Aeronautics and Astronautics, Beijing, China, in 1987.

Since 1996, he has been with the School of Mechanical Engineering, Purdue University, Lafayette, IN, and was promoted to an Associate Professor in 2002 and a Full Professor in 2007. He is one of the Kuang-piu Professors with the Zhejiang University, Zhejiang, China. His research interests include the design and control of intelligent high performance coordinated control of electromechanical/hydraulic systems, optimal adaptive and robust control, nonlinear observer design and neural networks for virtual sensing, modeling, fault detection, diagnostics, and adaptive fault-tolerant control, and data fusion. He has been actively involved in various technical professional societies such as ASME and IEEE, as reflected in his various posts as the organizer/chair of numerous sessions, the member of the International Program Committee of a number of IEEE, ASME, and IFAC conferences that he has served during the past several years. He was the chair of the Adaptive and Optimal Control panel from 2000 to 2002 and the chair of the Fluid Control panel of the ASME Dynamic Systems and Control Division (DSCD) from 2001 to 2003, and currently serves as the vice-chair of the Mechatronics Technical Committee of ASME DSCD that he initiated in 2005. He was a Technical Editor of the IEEE/ASME TRANSACTIONS ON MECHATRONICS from 2001 to 2005 and currently an Associate Editor of the ASME Journal of Dynamic Systems, Measurement, and Control.

Dr. Yao was a recipient of the Faculty Early Career Development (CAREER) Award from the National Science Foundation (NSF) in 1998 for his work on the engineering synthesis of high performance adaptive robust controllers for mechanical systems and manufacturing processes, a Joint Research Fund for Overseas Young Scholars from the National Natural Science Foundation of China (NSFC) in 2005, and the O. Hugo Schuck Best Paper (Theory) Award from the American Automatic Control Council in 2004 and the Outstanding Young Investigator Award of ASME Dynamic Systems and Control Division (DSCD) in 2007.

Jian Cao received the B.Eng. degree in fluid power transmission and control from the Inner Mongolia University of Science & Technology, Baotou, China, in 2002.

He is currently a candidate for Ph.D. in the State Key Laboratory of Fluid Power Transmission and Control, Zhejiang University, Hangzhou, China. His research interests include fluid power transmission and control, mechatronic control, etc.